

Electronic supplementary information

New insights into the electron transfer mechanism within flavohemoglobins: tunnelling pathways, packing density, thermodynamic and kinetic analyses

Emna El Hammi,^a Chantal Houée-Lévin,^a Jan Řezáč,^b Bernard Lévy,^a Isabelle Demachy,^a Laura Baciou*^a and Aurélien de la Lande^{*a}

^a Laboratoire de Chimie Physique – CNRS UMR 8000. Université Paris-Sud. Bât. 349-350, Campus d'Orsay. 15, avenue Jean Perrin, 91405 Orsay Cedex. France Fax: +33 169 15 61 88 ; Tel: +33 169 15 73 98; E-mail:aurelien.de-la-lande@u-psud.fr; laura.baciou@u-psud.fr

^b Institute of Organic Chemistry and Biochemistry, Academy of Sciences of the Czech Republic and Center for Biomolecules and Complex Molecular Systems, Flemingovo nam. 2, 166 10 Prague 6, Czech Republic.

Protein expression and purification

FlavoHb of *R. eutropha* was expressed in *E. coli* BL21 strains and purified as described previously (El Hammi et al. 2011 Biochemistry). Static absorption spectrum was recorded at room temperature using an Uvikon dual-beam spectrophotometer. The sodium dithionite-reduced minus oxidized difference of absorption spectra were recorded between 350 and 650nm. Concentrated and purified FHP (80µM) was dialyzed overnight against 10 mM Formiate buffer. The anaerobic samples to be irradiated (typically 300 µl) contained 20 µM of FHP in formiate buffer (10 mM) N₂O-saturated. Experiments were made in triplicate.

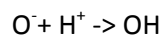
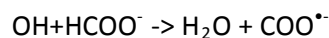
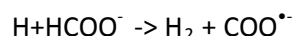
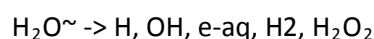
Pulse radiolysis.

Pulse radiolysis measurements were performed as described elsewhere. Free radicals were generated by the application into an N₂O-saturated aqueous solution of a 0.2-0.8 µs pulses of high energy electrons (*ca.* 4 MeV) from the linear accelerator located at the Institut Curie, Orsay, France. Under such conditions, the radicals generated by water radiolysis are converted into carboxylate radicals.

The doses per pulse were calibrated from the absorption of the thiocyanate radical (SCN)^{2•-} obtained by radiolysis of the thiocyanate ion in N₂O-saturated solution ([SCN⁻] = 10⁻² M, G((SCN)^{2•-}) = 0.55 µmol. J⁻¹, ε₄₇₂ nm = 7580 M⁻¹ cm⁻¹). The dose varies linearly with the pulse length, for instance a dose of *ca.* 5 Gy per pulse (0.2 µs long) resulted in *ca.* 2.8 µM of O₂^{•+}.¹ Reactions were followed spectrophotometrically, using a Hamamatsu SuperQuiet xenon-mercury lamp (150 W) between 310

and 750 nm or a tungsten lamp between 450 and 750 nm, at 20 °C in a 2 cm path length fused silica cuvette. The Xenon lamp was not submitted to a surtension. In all the pulse radiolysis experiments, a cut-off filter cutting all wavelengths below 320 nm was positioned between the lamp and the cuvette. Kinetic traces were analyzed using a Levenberg-Marquardt algorithm from the Kaleidagraph® software package (Synergy Software).

$\text{CO}_2^{\bullet-}$ radicals was generated during the scavenging by formate of the radiolytically produced hydroxyl radical, $\text{HO}^{\bullet-}$.²



The kinetic traces induced by a single pulse were obtained from measurements done at individual wavelengths between 400 and 650 nm.

Theoretical modeling

Various computational approaches are employed in this study: hybrid DFT/MM calculations for geometry optimizations of the heme and of the flavin cofactors as well as classical molecular dynamics simulations (MDS) for ET pathway analysis. Finally a combination of DFT and classical MDS for the evacuation of the driving force and reorganization energy is used.

Structure preparations: The starting structure of flavoHb is the crystallized form of the flavohemoglobin from *R. Eutropha* resolved at 1.75 Å (Protein Data Bank entry: 1CQX).³ A phospholipid is present in the distal pocket of the heme group. The protein was hydrogenated with the HBUILD module of the CHARMM package (version 35)⁴ and solvated in a box of 90x90x80 Å³ of flexible SPC water molecules.⁵ Sodium counter-ions were added to ensure electrical neutrality. The molecular systems were then relaxed by 1ns of molecular dynamics simulations and subsequent geometry optimizations to provide the starting geometries for DFT/MM optimizations and classical MDS-PM analysis.

QM/MM computations: we use the CUBY framework developed by Řezáč *et al.* to perform all the hybrid DFT/MM computations. Cuby interfaces the MM software CHARMM with the DFT program deMon2k.⁶ The DFT computations are realized with the OPBE⁷ functional in the unrestricted formalism with empirical corrections to account for dispersion effects (except on iron for which no parameters are available). A double dzeta with polarization functions basis set adapted for GGA functionals (DZVP-GGA) has been used on all atoms. The Dunning auxiliary basis sets GEN-A2 (for C, H and O) and GEN-A2* (for Fe and N, the star denotes the inclusion of f and g auxiliary functions) have been employed to expand the auxiliary electronic densities as employed in the so-called auxiliary DFT framework.⁸ An adaptive DFT grid of fine accuracy⁹ has been used for the numerical evaluations of the XC energy and potential and a multipolar expansion scheme has been employed to evaluate the DFT long range Coulomb integrals.¹⁰ Population analysis of the DFT electronic densities are realized according to the iterative Hirshfeld scheme¹¹ (HPA-I) recently implemented in deMon2k. The HPA-I cycles were repeated until the atomic charges variation were below 0.0005 between two cycles.

The QM/MM protocol follows a subtractive scheme with electrostatic embedding which is achieved through the inclusion in the DFT calculation of the environmental point charges of the MM atoms situated in less than 10 Å from the QM atoms. The QM/MM boundaries are treated with the link atom technique.¹² The DFT/MM geometry optimizations are performed on MM optimized structures keeping frozen the atoms situated beyond a distance of 10 Å from the QM atoms. When optimizing the iron center the quantum region includes the entire porphyrin (including the propionate groups), the metal ion and the His85 residue, that was cut at the level of the C_α-C_β bond. On the other hand when optimizing the flavin, the QM partition includes the isoalloxazine portion and the entire ribitol tail.

Pathway model and Packing Density analysis: 5ns of classical MDS have been realized within the Langevin approach and a time step of 0.5fs. The temperature was set to 300K. Snapshots were extracted from the MDS trajectories every 100 fs and then pruned to conserve only the residues suspected to be directly involved in the ET pathways. These are the Ile82, Ala82, Asn83, Lys84, His85, Ala86, Ser87, Leu88, Tyr190, Gln207, Glu394, Val395, Phe396 residues as well as the FAD and heme prosthetic groups. The phospholipid was also included in the pruned geometries. Finally all the water molecules whose oxygen atoms were localized within 8Å of the heme propionate A group were included in the PM and PD analysis.

DFT+MM computations: The driving force and the reorganization energy $\text{FAD}_{\text{red}} + \text{Fe(III)} \rightarrow \text{FAD}_{\text{ox}} + \text{Fe(III)}$ reactions were calculated following the approach detailed by Blumberger and co-workers (see for example Ref) Both the $\text{FADH}^{\cdot} \rightarrow \text{FADH}^{+}$ and the $\text{FAD}^{-} \rightarrow \text{FAD}$ oxidations are investigated. The inner-

sphere contributions are obtained from single point computations performed on the different cofactors optimized at DFT/MM level (see above). The outer-sphere contributions are obtained using the Linear Response Approximation expressions. First the vertical energy gap between the initial ($\text{Fe(III)}/\text{FAD}_{\text{red}}$) and the final ($\text{Fe(II)}/\text{FAD}_{\text{ox}}$) redox states is sampled from 5.4 ns MDS from Brownian MDS (using the Langevin approach) realized on the initial and final. Only the last 4.4ns were used for data accumulation.

$\Delta E^{\text{init}} = E_{\text{final}}^{\text{init}}(t) - E_{\text{init}}^{\text{init}}(t)$ is computed along an MDS performed on the initial state

$\Delta E^{\text{final}} = E_{\text{final}}^{\text{final}}(t) - E_{\text{init}}^{\text{final}}(t)$ is computed along an MDS performed on the final state.

E_b^a denotes the MM potential energy in state b computed on a molecular geometry corresponding to belonging to a NVT statistical ensemble corresponding to state a . To avoid any double counting with the inner-sphere contributions, the intra-molecular MM energy of the redox cofactors are retrieved from E_b^a . The outer-sphere contributions of driving force and of the reorganization energies are then computed according to:

$$\Delta G_o = \frac{1}{2} (\langle \Delta E^{\text{init}} \rangle + \langle \Delta E^{\text{final}} \rangle)$$

$$\lambda_o = \frac{1}{2} (\langle \Delta E^{\text{init}} \rangle - \langle \Delta E^{\text{final}} \rangle)$$

Table 1: Force field charges for the Fe(II) (triplet) and Fe(III) (quadruplet) complexes derived from the iterative Hirshfeld charges obtained on the OPB/MM optimized structure. The atom labeling corresponds to the heme atom definitions of the CHARMM force field.

| | Fe(II) | Fe(III) | | Fe(II) | Fe(III) | | Fe(II) | Fe(III) |
|------|---------|---------|------|---------|---------|---------------|---------|---------|
| FE | 1.204 | 1.5343 | CAA | -0.1861 | -0.2217 | CMD | -0.5177 | -0.5452 |
| NA | -0.543 | -0.6118 | HAA1 | 0.1308 | 0.1426 | HMD1 | 0.1473 | 0.168 |
| NB | -0.5543 | -0.6222 | HAA2 | 0.1135 | 0.1331 | HMD2 | 0.1665 | 0.1818 |
| NC | -0.544 | -0.6102 | CBA | -0.5963 | -0.5804 | HMD3 | 0.158 | 0.1865 |
| ND | -0.5748 | -0.6439 | HBA1 | 0.1564 | 0.1577 | CAD | -0.1817 | -0.223 |
| C1A | 0.2972 | 0.3117 | HBA2 | 0.1677 | 0.1629 | HAD1 | 0.138 | 0.1494 |
| C2A | -0.0342 | 0.0167 | CGA | 1.0229 | 1.0144 | HAD2 | 0.121 | 0.1438 |
| C3A | 0.0203 | 0.0453 | O1A | -0.8999 | -0.8774 | CBD | -0.5889 | -0.5663 |
| C4A | 0.2861 | 0.3123 | O2A | -0.9019 | -0.8863 | HBD1 | 0.1533 | 0.1564 |
| C1B | 0.2888 | 0.3177 | CMB | -0.5218 | -0.5338 | HBD2 | 0.1608 | 0.1563 |
| C2B | 0.0795 | 0.0873 | HMB1 | 0.1461 | 0.1547 | CGD | 1.014 | 1.0023 |
| C3B | -0.1253 | -0.0818 | HMB2 | 0.15 | 0.1566 | O1D | -0.895 | -0.8865 |
| C4B | 0.3259 | 0.3396 | HMB3 | 0.1584 | 0.1678 | O2D | -0.917 | -0.8675 |
| C1C | 0.2672 | 0.2882 | CAB | -0.0153 | -0.0445 | <i>His85:</i> | | |
| C2C | 0.0341 | 0.0598 | HAB | 0.1042 | 0.1209 | CA | 0.2245 | 0.2366 |
| C3C | -0.1386 | -0.097 | CBB | -0.3938 | -0.3478 | CB | -0.6114 | -0.6247 |
| C4C | 0.3065 | 0.3347 | HBB1 | 0.1499 | 0.1494 | HB1 | 0.2078 | 0.2154 |
| C1D | 0.2745 | 0.3104 | HBB2 | 0.1314 | 0.1419 | HB2 | 0.1743 | 0.1864 |
| C2D | 0.0366 | 0.0649 | CMC | -0.503 | -0.5262 | ND1 | -0.4959 | -0.4871 |
| C3D | -0.038 | 0.0238 | HMC1 | 0.1289 | 0.1441 | HD1 | 0.4952 | 0.5111 |
| C4D | 0.3103 | 0.3265 | HMC2 | 0.1307 | 0.1522 | CG | 0.3414 | 0.3618 |
| CHA | -0.4011 | -0.3737 | HMC3 | 0.1616 | 0.1817 | CE1 | 0.2205 | 0.2507 |
| HA | 0.1787 | 0.1992 | CAC | -0.0238 | -0.058 | HE1 | 0.0676 | 0.0751 |
| CHB | -0.4038 | -0.3992 | HAC | 0.0785 | 0.0964 | NE2 | -0.4321 | -0.5231 |
| HB | 0.1562 | 0.1707 | HD | 0.1607 | 0.1778 | CD2 | -0.1338 | -0.1123 |
| CHC | -0.4436 | -0.4319 | CMA | -0.5243 | -0.5439 | HD2 | 0.1316 | 0.1367 |
| HC | 0.1521 | 0.1713 | HMA1 | 0.1569 | 0.1702 | | | |
| CHD | -0.4186 | -0.4086 | CBC | -0.3574 | -0.296 | | | |
| HMA2 | 0.1673 | 0.1848 | HBC1 | 0.1574 | 0.1584 | | | |
| HMA3 | 0.1419 | 0.1555 | HBC2 | 0.1314 | 0.1462 | | | |

-
- ¹ G. V. Buxton, C. R. Stuart *J Chem Society-Faraday Trans* 1995, **91**, 279.
- ² J.W.T. Spinks, R. J. Woods, Introduction to radiation chemistry. 1990 Wiley Interscience, New York
- ³ U. Ermler, R. A. Siddiqui, R. Cramm, B. Friedrich, *EMBO J.* 1995, **14**, 6067.
- ⁴ B. R. Brooks et al. *J. Comput. Chem.* 1983, **4**, 187.
- ⁵ Y. Wu, H. L. Tepper, G. A. Voth, *J. Chem. Phys.* 2006, **124**, 024503.
- ⁶ Koster, A. M.; Geudtner, G.; Calaminici, P.; Casida, M. E.; Dominguez, V. D.; Flores-Moreno, R.; Gamboa, G. U.; Goursot, A.; Heine, T.; Ipatov A.; Janetzko F.; Martin del Campo, J.; Reveles, J. U.; Vela, A.; Zuniga-Gutierrez, B.; Salahub, D. R.; *deMon2k*, Version 3, **2011**, The deMon developers, Cinvestav, Mexico City.
- ⁷ N. C. Handy, A. Cohen, *J. Mol. Phys.* 2001, **99**, 403.
- ⁸ A. M. Köster, J. U. Reveles, J. M. del Campo, *J. Chem. Phys.* 2004, **121**, 3417.
- ⁹ M. Krack, A. M. Köster, *J. Chem. Phys.* 1998, **108**, 3226.
- ¹⁰ A. M. Köster, *J. Chem. Phys.* 2003, **118**, 9943.
- ¹¹ P. Bultinck, C. Van Alsenoy, P. W. Ayers, R. Carbó-Dorca, *J. Chem. Phys.* 2007, **126**, 144111.
- ¹² M. J. Field, P. A. Bash, M. Karplus, *J. Comput. Chem.* 1990, **11**, 700